Shape primed AC-electrophoretic microrobots

Florian Katzmeier, Friedrich C. Simmel*

Physics Department E14, TU Munich, D-85748 Garching, Germany

*To whom correspondence should be addressed; E-mail: simmel@tum.de

Second-order electrokinetic flow around colloidal particles caused by concentration polarization electro-osmosis can be utilized to controllably move asymmetric particle dimers in AC electrical fields. To demonstrate this actuation mechanism, we created particle dimers from micron-sized silica spheres with sizes $1.01\,\mu$m **and** $2.12\,\mu$m **by connecting them with DNA linker molecules. The dimers can be steered along arbitrarily chosen paths within a 2D plane by controlling the direction of the AC electric field in a fluidic chamber with the joystick of a gamepad. Further utilizing induced dipole-dipole interactions, we demonstrate that particle dimers can be used to controllably pick up monomeric particles and release them at any desired position, and also to assemble several particles into groups. Systematic experiments exploring the dependence of the movement direction and velocity on buffer composition, frequency, and field strength further elucidate the underlying physical mechanism, and provide operational parameter ranges for our micro robotic swimmers which we termed 'SPACE-bots'.**

Introduction

Microscopic machines operate under fundamentally different conditions compared to macroscopic machines as the relative strength of the forces acting on them changes with the size of a system. This renders design strategies usually employed for macroscopic machines ineffective at a microscopic scale. [1] In particular, propulsion mechanisms such as paddling used to propel macroscopic machines are ineffective at a micro-scale where Reynolds numbers are low and fluid friction dominates over inertia. [2] However, at such scales, other mechanisms such as thermophoresis, chemophoresis, or electrophoresis [3, 4, 5] become relevant, which in turn are ineffective at a macro-scale. It is therefore advantageous to understand, control and employ such mechanisms when engineering microscopic machines. In this work, we introduce a novel type of electrophoretic microswimmers inspired by recent insights into the electrokinetic flow around colloidal particles in AC electric fields. [6, 7, 8]

It is well known that anisotropic and asymmetric microscopic particles undergo propulsion in AC electric fields. Metallo-dielectric Janus particles, for instance, migrate perpendicularly to the direction of the electric field. [9] Further, asymmetric colloidal dimers [10] and also metallo-dielectric Janus particles [11] placed on an electrode and subjected to a vertical electric field are propelled perpendicularly to the electric field in a random direction in the 2D plane defined by their current orientation. Within this setup, magnetic fields have been used in combination with ferromagnetic metallo-dielectric Janus particles [12] and ferromagnetic asymmetric colloid dimers [13] to introduce maneuverability. Further, it has been demonstrated that metallo-dielectric Janus particles can be used to transport other dielectric particles. [14, 15, 12]

These propulsion mechanisms either rely, as in the case of polarizable metallo-dielectric Janus particles, on inducted charge electro-osmosis/phoresis [16, 17], or, in the case of asymmetric particles, on the electrohydrodynamic interplay between electrode and particle [18, 19]. Here

we introduce a novel strategy, based on the recently discovered mechanism of concentration-polarization electro-osmosis [6, 7, 8], that requires neither polarizable particles nor a nearby electrode. We show that asymmetric microscopic particles undergo alignment and directed propulsion parallel to the field lines of an applied AC-electric field far away from the electrodes. We name this unusual propulsion mechanism relying on particle asymmetry ”Shape-Primed AC-Electrophoresis (SPACE)” to distinguish it from traditional electrophoresis, which works in DC-electric fields and is usually shape-independent [20]. Furthermore, we demonstrate that such Shape-Primed AC-Electrophoretic microrobots (SPACE-bots) can be precisely maneuvered within a relatively uncomplicated setup without additional magnetic forces by simply controlling the direction of the AC-electric field in a 2D plane. Within this framework, we developed a strategy to pick up, transport, and release spherical cargo particles with our microrobots based on our understanding of the relevant electric and hydrodynamic interactions at a microscopic scale. Finally, we explore the dependence of the microrobots' migration speeds on the electric field strength, frequency, and buffer composition and find reasonably good agreement with theoretical predictions [6, 7].

Results

It is known that the axial-symmetric fluid flow shown in Fig. 1B arises around a spherical particle when subjected to an AC electrical field in a low ionic strength aqueous medium. Fluid flows towards the particle in the direction of the electric field and is repelled perpendicularly to the electric field. [6, 7] We expected that for an asymmetric dimeric particle an asymmetric flow would arise as proposed in Fig. 1C that would lead to the propulsion of the particle. Further, a dimeric particle will also align with the external electric field as shown in Fig. 1C and Fig. 1A due to an induced electric dipole. In combination with the propulsion this leads to a directed

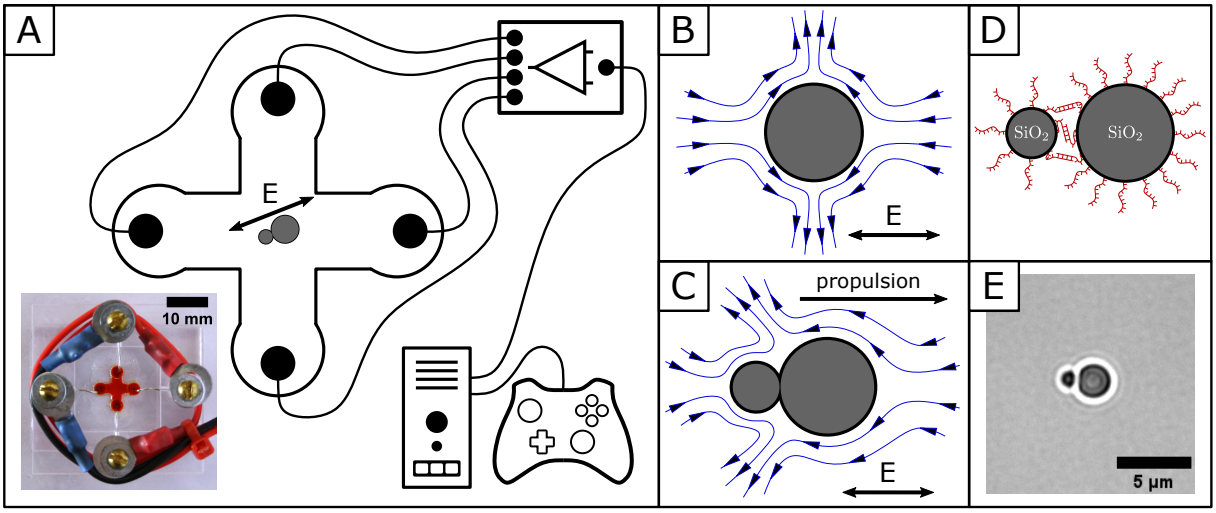

Figure 1: (A) Scheme and photograph of our experimental setup that enables control of the direction and amplitude of an AC-electric field in a microscopy chamber. A dimer is drawn in the center of the cross-shaped fluidic chamber, which aligns with the externally applied AC-electric field through an induced dipole. For visualization, the fluidic chamber in the photograph is filled with a red dye. (B) Electrokinetic flow around a spherical particle arising in an AC-electric field. (C) Expected electrokinetic flow around an asymmetric particle dimer in an AC-electric field, which results in directed propulsion. (D) DNA modified colloids form a dimer through DNA hybridization. (E) Microscopy image of a particle dimer.

motion along the field lines of the external electric field. The motion of such shape-primed AC-electrophoretic microrobots (SPACE-bots) can thus be easily controlled externally by changing the direction and strength of the external AC-electric field.

In order to be able to control the AC-electric field, we designed the sample chamber shown in Fig. 1A, in which two microfluidic channels equipped with platinum electrode pairs at their inlets intersect in the center. The electric field at the intersection is a superposition of the fields applied to each of the channels. Hence, the direction and strength of the field at the intersection can be controlled by applying different electric field strengths to the channels.

We created two electric signals with the sound card of a computer, which were then amplified in two stages using custom-built amplifiers before applying them to the microchannels. With our setup we can apply AC voltages with an amplitude of up to $305\,$V which translates to a electric field amplitude of approximately $60\,$mV$/$µm in the center of our chamber. We furthermore programmed a python script to control the amplitude of the electric signals via the XY-deflection of the analog joystick of a gamepad (an Xbox Controller) which is conventionally used to play video games. As a result, the direction and amplitude of the AC electric field in our sample chamber and thereby the movement of our microscale SPACE-bots can be directly controlled with a joystick while imaging them with a microscope. This gives the experimenter intuitive control over the SPACE-bot's movement. We also included the possibility to change the field frequency to predefined values $250\,$Hz, $450\,$Hz, $750\,$Hz, and $950\,$Hz by pressing the buttons available on the controller. More pictures of the setup together with more detailed information on its design and manufacturing can be found in the Supplementary Materials.

Our SPACE-bots are composed of two different-sized silica spheres with diameters $1.01\,$µm and $2.12\,$µm that are linked to each other via complementary DNA strands (see Fig. 1D). Each particle type was modified with single-stranded DNA, whose sequence was chosen comple-

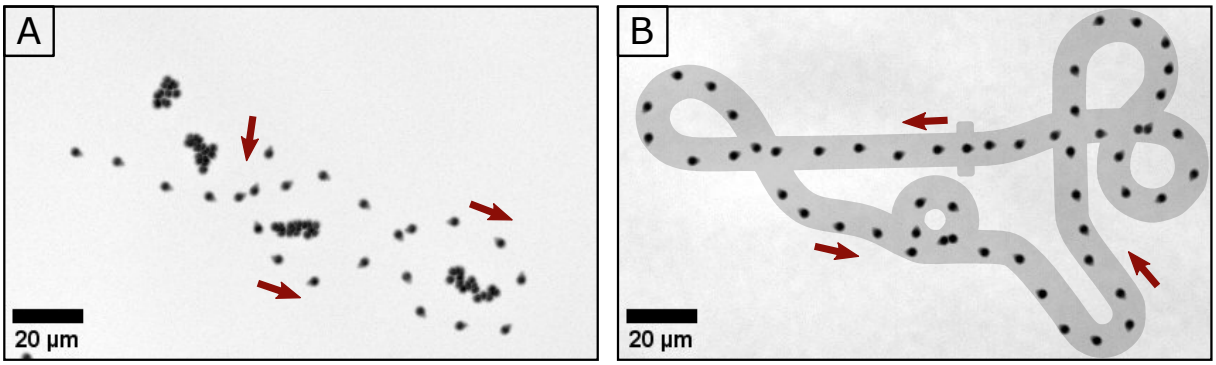

Figure 2: (A) By applying joystick-controlled AC voltages ($V_{pp} = 610\,\mathrm{V}, f = 250\,\mathrm{Hz}$) the SPACE-bot is maneuvered through a slalom course around stationary monomer particles. The image shows an overlay of successive frames of a recorded microscopy video. Notably, the monomer particles appear as particle clouds due to Brownian motion, but they do not respond the applied AC field. The direction of motion of the SPACE-bot is indicated with red arrows. (B) A SPACE-bot is maneuvered along a race track adopted from a well-known computer game. The image shows an overlay of successive frames of a recorded microscopy video and the racetrack.

mentary to that of the strands on the other particle type. When mixed in $4\,$mM $MgCl_2$, the different-sized silica spheres can bind to each other via DNA duplex formation. A microscopy image of a assembled SPACE-bot is shown in Fig. 1E. For our experiments we diluted our SPACE-bots in $50\,$µM Tris-buffer (pH 8.4) supplemented with $5.2\,$µM $MgCl_2$. A detailed description of the synthesis and sample preparation is given in the Materials and Methods section.

In Fig. 2 we explore the maneuverability of our SPACE-bots. We usually found a collection of mainly monomers and dimers in our sample, but also small amounts of multimers. All dimers (SPACE-bots) collectively move in the direction of the field since they are subject to the same AC field-induced electrokinetic fluid flow while the monomers remain stationary. In our experiments, we usually focused on a single SPACE-bot. To demonstrate maneuverability, we recorded a microscopy video where we steered a SPACE-bot along a slalom course around islands of monomeric particles (see first part of Movie 1). Fig. 2A shows an overlay image of the recorded video, for which we computed the minimum intensity of a selection of

frames. The monomeric particles appear as clouds, since they are subject to Brownian motion. The direction of motion of the SPACE-bot is indicated with red arrows. We found a slight drift in our microscopy videos which we attribute to bulk fluid motion generated at the electrodes. We corrected the drift in the microscopy videos by tracking several of the monomeric particles and shifting the recorded video by their average displacement. Details on video processing are given in the Methods section.

We also recorded a microscopy video, in which we maneuvered a SPACE-bot along a racetrack. For this purpose, we printed the racetrack on a cling film and attached it with tape to the screen of the computer controlling the microscope. We then maneuvered a SPACE-bot along the racetrack while recording a video (see second part of Movie 1). Fig. 2B shows an overlay of video images and the racetrack. No drift correction had to be applied to the video, as in this case the drift was corrected intuitively directly by the human operator.

We found that the SPACE-bots can be readily used to pick up, transport, and release other, *monomeric* cargo particles. For this purpose, we utilize both electric and hydrodynamic forces between a SPACE-bot and a cargo particle. Fig. 3A shows a microscopy image of a SPACE-bot approaching a cargo particle. The direction of motion is again indicated with a red arrow and the cargo particle is labeled with a blue arrow. The fluid flow around the SPACE-bot and the cargo particle is illustrated in the sketch above the microscopy image. Fluid flows towards both particles in the direction of the electric field and is repelled perpendicularly to the electric field. The SPACE-bot and the cargo particle drift in the fluid flow caused by each other which results in an attractive interaction for the illustrated configuration. When in direct contact, the SPACE-bot is stuck to the cargo particle via induced dipole-dipole forces (see Fig. 3B). We then maneuvered the SPACE-bot together with the loaded cargo particle around another monomeric particle. At any point in time the external field induces an electric dipole in the cargo particle as well as in

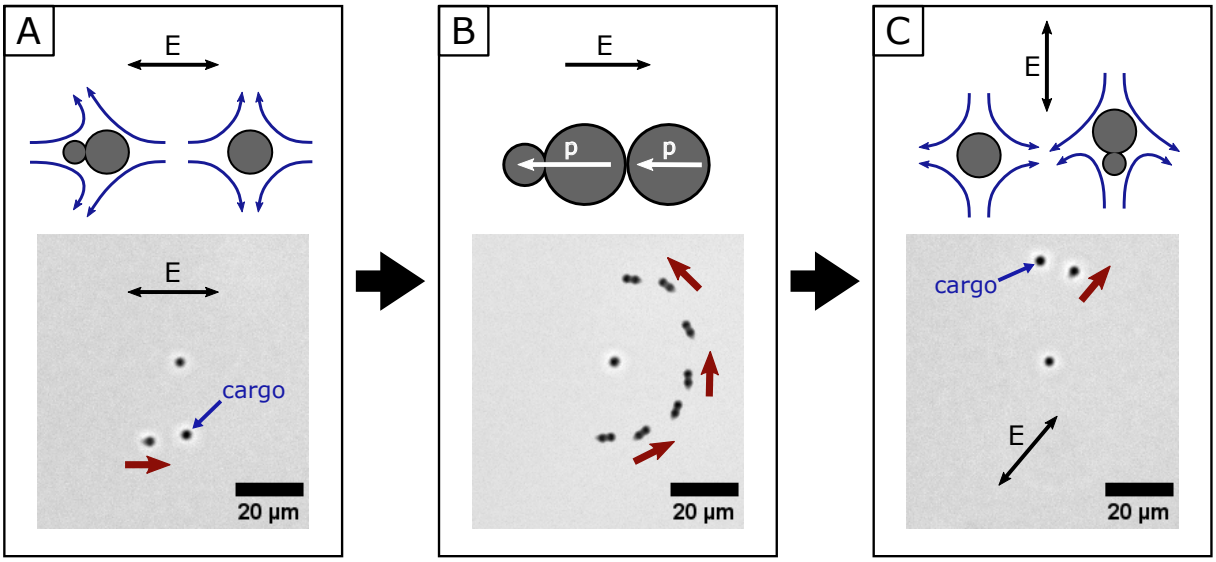

Figure 3: Mechanistic illustration of cargo pick up, transport and release. (A) A SPACE-bot approaches a cargo particle. The direction of motion of the SPACE-bot is indicated with an red arrow. The cargo particle is labeled with a blue arrow. The direction of the AC-electric field is indicated with a black double arrow. The fluid flow arising around the SPACE-bot and the cargo particle is illustrated with curved blue arrows in the sketch above and leads to an attraction. (B) A SPACE-bot sticks to a cargo particle via induced dipole dipole forces. Both are maneuvered around an other monomeric particle. The induced dipole moments at an instance in time are indicated with white arrows in the sketch above. The electric field is indicated with a black arrow. (C) A cargo particle is released from a SPACE-bot by a quick change in direction of the external electric field. The fluid flow arising around the SPACE-bot and the cargo particle now leads to repulsion.

the SPACE-bot. Both induced dipoles point in the same direction during a period of the external AC-electric field which results in a near-field attraction of the particles. This mechanism is well known and results in particle chain formation in crowded colloidal suspensions. [21, 22, 6] For further analysis, we corrected the drift in the corresponding microscopy video by tracking the monomeric *non-cargo* particle and shifting the recorded video by its displacement. This makes the non-cargo particle appear as a single particle in the shown overlay image. Cargo release (shown in Fig. 3C) is achieved by switching off the electric field, changing the frequency from 250 Hz to 750 Hz, and then applying an AC electric field oriented roughly perpendicularly to the previous field. The resulting particle configuration is illustrated in the sketch above the microscopy image. The fluid repelled from the particles' equator perpendicularly to the electric field results in a repulsion of the particles. As soon as the SPACE-bot has moved sufficiently far away from the cargo particle, the frequency is set back to 250 Hz, which re-establishes electrokinetic control over the SPACE-bot. We found that changing the frequency makes it easier for the experimenter to execute cargo release. We assume that the induced dipole-dipole force decreases in strength relative to the force exerted by the fluid flow at higher frequencies. A video of the cargo transport process is shown in the third part of Movie 1. We also demonstrate that the outlined strategy can be used to assemble three monomeric particles into a particle chain (see last part of Movie 1).

Having established a novel approach for the manipulation of micro-swimmers based on asymmetric microparticle dimers, we characterized the parameter dependence of their migration speed in greater detail. We suspected the migration speed to scale similarly as the strength of the fluid flow around spherical particles, which is known to depend on the electric field strength, its frequency, the buffer composition and the surface charge of the particles, which in turn depends on the pH of the buffer. As a second-order phenomenon with respect to the applied elec-

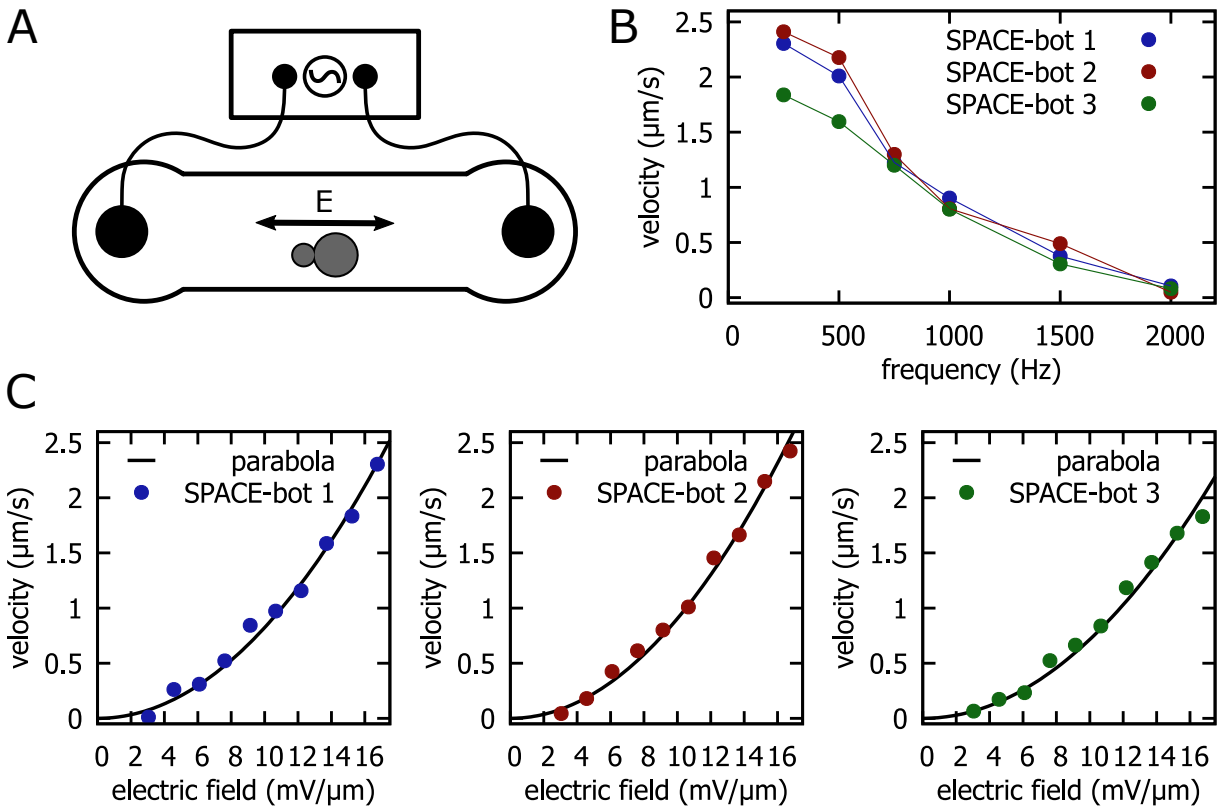

Figure 4: (A) Simplified setup to characterize the migration speed of SPACE-bots. An AC-electric field is applied to a linear microscopy channel containing SPACE-bots. (B) Migration speed of three different SPACE-bots at a constant electric field amplitude of $16.75\,\mathrm{mV/\mu m}$ and varying frequency. The colored lines are a guide for the eye. (C) Migration speed of three different SPACE-bots at a constant frequency of $250\,\mathrm{Hz}$ and varying electric field amplitude. The black lines are parabolas ($v = \lambda E_0^2$) fitted to the migration speed data.

tric field, we expect the migration speed v to scale as $v \propto E_0^2$ with the field amplitude E_0. [6, 7] We furthermore expected that for increasing frequencies the migration speed would decrease in the same way as the fluid flow around spherical particles, which occurs around the characteristic frequency $f_{\text{cr}} = \frac{2}{\pi} \frac{D^+ D^-}{R^2 (D^+ + D^-)}$ [23, 24, 6, 7]. Here, D^- and D^+ denote the diffusion coefficients of the buffer ions Cl^- and Tris$-H^+$, which are $D^- = 2000\,\mu\text{m}^2/\text{s}$ and $D^+ = 800\,\mu\text{m}^2/\text{s}$ at $T = 20\,°\text{C}$. [25]. R is the particle radius which we will interpret as the typical size of our SPACE-bots. f_{cr} can be understood as a characteristic frequency that is defined by the time required for ions to diffuse around a spherical particle. For our experimental settings, we obtain the range $[150\,\text{Hz}, 1400\,\text{Hz}]$ for f_{cr}, when using the radius of the smaller particle ($R = 0.51\,\mu\text{m}$) for the upper bound and the combined radius of both particles ($R = 1.57\,\mu\text{m}$) for the lower bound.

We measured the migration speed of three different SPACE-bots for several voltages and frequencies to verify the above hypothesis. To this end, we employed the setup shown in Fig. 4A where SPACE-bots are placed in a linear microchannel with two electrodes at its opposite inlets. As before, we prepared the SPACE-bots in $50\,\mu\text{M}$ Tris-buffer titrated to a pH 8.4 by the addition of HCl and supplemented with $5.2\,\mu\text{M}$ $MgCl_2$. We then recorded microscopy videos of the migration of the three SPACE-bots while applying different frequencies and voltages. From the start and end positions of the SPACE-bots, we computed the distances covered and from these the average migration speeds. We also measured the speed of a monomeric particle as a reference. The corresponding measurements are listed in Tables S9-S11. Fig. 4C shows plots of the migration speeds versus the applied electric field amplitude at a constant frequency of $250\,\text{Hz}$. As shown, the experimental migration speeds are well described by a quadratic fit $v = \lambda E_0^2$. In Fig. 4B, the frequency dependence of the migration speeds of the three swimmers is plotted for a constant electric field amplitude of $16.75\,\text{mV}/\mu\text{m}$, which shows the expected decrease in the frequency range $[150\,\text{Hz}, 1400\,\text{Hz}]$.

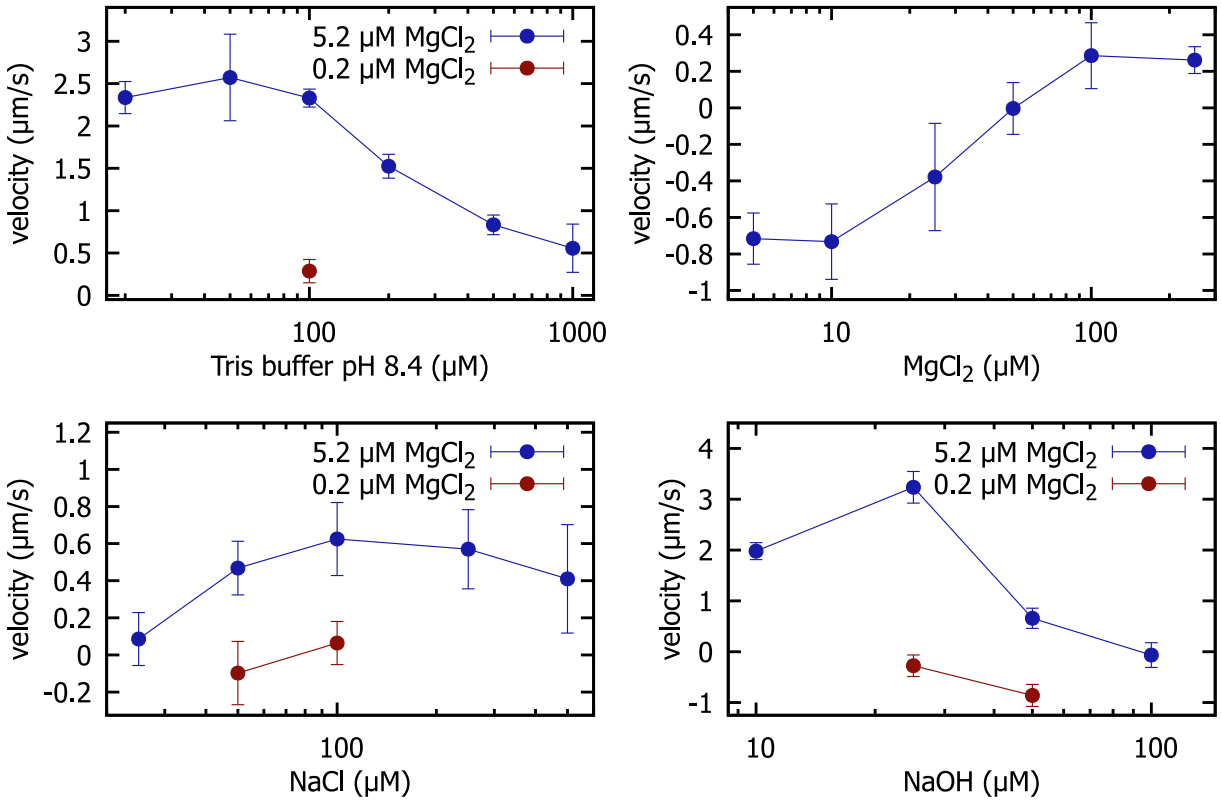

Figure 5: SPACE-bot velocities at a constant electric field amplitude of $16.75\,\mathrm{mV/\mu m}$ and constant frequency of $250\,\mathrm{Hz}$ for various buffer conditions. Blue data points indicate measurements with $MgCl_2$ supplemented to the buffer, while red data points correspond to measurements without supplemented $MgCl_2$. Each data point is the average of at least 5 velocity measurements of different SPACE-bots, error bars indicate the corresponding standard deviations. Data points with negative velocities correspond to SPACE-bots moving backward, which we defined as a movement with the smaller particle in front.

While the overall dependence of the migration speed on electric field strength and frequency is most likely independent of the type of colloids used, we expect the migration speed to depend on their surface properties. In the case of our microswimmer particles, the hydrodynamic flow around them is caused by ion-selective surface conduction in the electrical double layer at their surface. The double layer is characterized by the electric surface potential (zeta potential), which depends on the ionic strength of the buffer and the surface charge of the particle. The flow is expected to be strongest for high surface potentials, which corresponds to conditions with large surface charge densities and low ionic strengths (< 1 mM). [6]

Lastly, we also characterized the buffer dependence of the migration speed of our SPACE-bots. We recorded microscopy videos of SPACE-bots prepared in buffers with different concentrations of Tris, NaCl and NaOH, each supplemented with a constant concentration of 5.2 µM $MgCl_2$. In addition, we tested Tris-buffer, NaCl and NaOH without any $MgCl_2$ and also in a solution containing exclusively $MgCl_2$. For each buffer composition, we recorded tracks of at least five SPACE-bots, and we took care that every video contained at least one spherical particle as a reference. As before, we measured the migration speed by marking the start and end position of the SPACE-bot and dividing the resulting distance by the elapsed time. We also measured the migration speed of all spherical particles in each microscopy video and used it as a reference.(see Methods for details) The results of these characterization experiments are listed in Tables S1-S8 and plotted in Fig. 5. Overall we find decreasing velocities for increasing monovalent salt concentrations, and the decrease falls roughly within the expected range (i.e., for concentrations < 1 mM). The details of the buffer dependence of the particle velocity are, however, convoluted. We find that supplementing our buffer with 5.2 µM $MgCl_2$ has a tremendous effect on the migration speed. For Tris buffer, we find an enhancement of the velocity when supplementing the buffer with 5.2 µM $MgCl_2$ (see red datapoint at 100 µM Tris buffer compared

to the blue datapoint above). Moreover, for NaOH, we find an even more striking effect when supplementing $MgCl_2$, where SPACE-bots move backwards in the absence of $MgCl_2$, while they move forward in its presence. Notably, when we use $MgCl_2$ alone, we find backward movement that changes to forward movement at higher concentrations. NaOH or $MgCl_2$ alone at low concentrations induce backward movement, while their combination induces forward movement. We find the highest migration speeds for NaOH and Tris buffer at pH 8.4, which we attribute to an increased surface charge caused by the elevated pH. As trace amounts of $MgCl_2$ appear to have an extreme effect on the migration velocity, we took special care to avoid any salt contamination in our samples (see Methods for details).

We suspect that the observed behavior relates at least in part to the strong interactions between the DNA on the colloid surface and Mg^{2+} ions [26]. Mg^{2+} are known to bind to the DNA backbone with an apparent dissociation constant of (0.65 ± 0.33) µM [27], which is well below the supplemented $MgCl_2$ concentration. The bound Mg^{2+} alters the effective charge and conformation of the DNA, which in turn affects the electrokinetic properties of the surface drastically. A more detailed mechanistic explanation of the observed behavior, however, seems difficult.

We would finally like to briefly comment on the requirement for asymmetric shapes for our microswimmers. According to the century-old theory by Smoluchowski, electrophoresis of non-polarizable colloids is shape-independent [20], which would result, in combination with the time reversibility of hydrodynamics at low Reynolds numbers, in no net movement in an AC-electric field. In the case of our SPACE-bots, however, a net movement is found, which is explained by the breakdown [28, 29] of Smoluchowski's linear theory for our experimental conditions, i.e., at low salt concentrations and high surface potentials. Asymmetrically shaped swimmers thus elicit an asymmetric fluid flow around them which leads to their directional propulsion.

Conclusion

We have introduced a novel approach towards precise AC electrophoretic manipulation of microswimmers, which provides unprecedented electrical control over two-dimensional movements. In contrast to other approaches for electrically driven swimmers, the utilization of concentration–polarization electroosmosis enables the use of in-plane electric fields to move the particles in the direction of the field lines (rather than perpendicular to them). The movement requires asymmetric particles with a surface charge, but the particles themselves do not have to be 'Janus'. In our case, two differently sized silica particles were connected using DNA linker molecules. As indicated by the joystick-controlled movements demonstrated in this work, our microswimmers are of immediate interest for micro-robotics. The SPACE-bots can move along arbitrarily chosen paths in 2D and thereby controllably pick up, release, and also assemble particles.

In future work, it is conceivable to utilize the AC electrophoretic manipulation mechanism to generate more complex functions. For instance, differently sized/shaped particles are expected to show a different frequency response, which could also be used to frequency-select only a fraction of the SPACE-bots. It is conceivable to let SPACE-bots assemble other microparticles into defined super-structures, potentially also other SPACE-bots. One of the challenges for future applications is the realization of operating conditions that are compatible with useful chemical or biochemical reactions (to assist assembly tasks), or even with biological entities, e.g., for the manipulation of bacteria or even mammalian cells.

Methods

Colloid modification

Carboxylated silica spheres with diameters 1.01 µm (Lot: SiO_2 – COOH-AR756-5ml) and 2.12 µm (Lot: SiO_2 – COOH-AR1060-5ml) were purchased from microParticles GmbH. We modified

the surface of the silica spheres by activating the carboxyl groups with 1-Ethyl-3-(3-dimethylaminopropyl) carbodiimide (EDC) and coupling them to amino-modified DNA. [30, 31] The colloids were reacted in 200 µL of 100 mM MES buffer (pH 4.8 adjusted with HCl and NaOH) containing 250 µM amino-modified DNA and 250 mM EDC (Merck: Art. No. E6383-1G) on a rotator at room temperature for 3 h. We used colloid concentrations of $11.35 \cdot 10^9$/mL and $50 \cdot 10^9$/mL of the 2.12 µm colloids and the 1.01 µm colloids, respectively, to account for the different surface areas of the colloids. The colloids were then washed and incubated extensively in borate buffer (boric acid adjusted to pH 8.2 with NaOH) and deionized water to get rid of remaining reaction components and to hydrolyze unreacted activated carboxyl groups. We avoided using buffers containing amino groups for washing as we wanted to preserve the negative surface charge of the colloids. An extended protocol with details on the washing procedure is given in the Supplementary Materials. Finally, the colloids were diluted to concentrations of $2.27 \cdot 10^9$/mL (2.12 µm colloids) and $10 \cdot 10^9$/mL (1.01 µm colloids) in deionized water, shock frozen in liquid nitrogen and stored at $-80\,^{\circ}$C.

Our two DNA strands are 60 nucleotides (nt) long and are each composed of a 30 nt long spacer region followed by a 30 nt region which is complementary to the corresponding region on the other strand. The spacer provides flexibility in the distance between the colloids where hybridization can take place. We designed our DNA sequences with NUPACK [32] such that they have no secondary structure. The oligonucleotides were purchased from Integrated DNA Technologies as dried pellets, their sequences are listed in the Supplementary information. We diluted our DNA strands in deionized water and stored them at $-20\,^{\circ}$C.

SPACE-bot assembly

We assembled our SPACE-bots by incubating concentrations of approximately $1.6 \cdot 10^9$/mL of each colloid with 4 mM $MgCl_2$ in a reaction volume of 25 µL for 45 min on a rotator. The above colloid concentration assumes that no colloids were lost in the above washing procedure. The reaction is stopped by rapid dilution of the sample by a factor of 1 to 1000 in deionized water. The sample is handled with special care as we found that shaking causes the SPACE-bots to disintegrate. For further use, we usually diluted our SPACE-bots again by a factor of 1 to 20 in a buffer of choice. The SPACE-bots were assembled freshly for every day of experiments.

Sample preparation

In initial experiments, we found a reduction in the migration speed after washing our pipette tips. We therefore suspected that the pipette tips contained trace amounts of divalent ions. In order to establish stable and reproducible behavior of the swimmers, we henceforth cleaned all pipette tips and the sample chamber with deionized water before usage. With every fresh pipette tip, we pipetted deionized water three times before pipetting an actual sample. We also washed all used reaction tubes with deionized water before usage, vortexed them and removed the deionized water again. For our screening experiments, we used commercial microscopy chambers purchased from ibidi (µ-Slide VI 0.4; Cat.No:80601). Before usage, the microscopy chambers were filled three times with deionized water and then blown dry with nitrogen gas.
For our experiments with Tris-buffer, we created a 50 mM stock solution at pH 8.4 by titrating Tris (Carl Roth: Art. No. 4855.2) with HCl. We avoided using NaOH in case of overshooting pH 8.4 as this would have resulted in an unknown concentration of additional NaCl in the buffer.

Video editing

We used ImageJ to edit our videos. We corrected the drift in the corresponding microscopy video by tracking the monomeric particles with the ImageJ plugin TrackMate [33] and shifting the recorded video by their displacement. Overlay images were created by computing the minimum intensity of a collection of frames from a microscopy video. We adjusted the contrast and brightness of our videos and images such that they appear alike. The final video editing was done with the freely available software Shotcut [34].

Data analysis

We marked the start and end positions of every SPACE-bot and reference particle in a video and saved the coordinates with the corresponding frame number. We also recorded the instantaneous orientations of every SPACE-bot, which lets us identify backward and forward movements. For that purpose, we used an ImageJ macro to automatize the data analysis. We computed the velocities of all SPACE-bots and reference particles by subtracting the y-coordinates of the start and end positions and dividing the result by the elapsed time. The elapsed time was extracted from the metadata of the corresponding video. We then computed the average velocity of all reference particles in a video and subtracted the velocity of every SPACE-bot in a video by the result, which gives us the corrected SPACE-bot velocities. The average and standard deviation are then computed from the corrected velocities of all videos with the same buffer conditions. All measured velocities and the recorded SPACE-bot orientations for our buffer characterization experiments are listed in the Supplementary Tables S1-S8.

In our frequency and electric field characterization experiments, we were interested in the response of a single SPACE-bot and reference particle. We, therefore, applied a simplified data analysis procedure and measured only the speed of the single SPACE-bot and reference particle in a video. The recorded measurements are listed in the Supplementary Tables S9-S11.

Setup design and operation

The design of our self-made sample chamber is inspired by that of Kopperger et al. [35]. Our sample chambers were milled from of a 5 mm thick PMMA sheet using a micro-milling machine. The bottom part of our microscopy chamber is a glass cover slide (Carl Roth: Art. No. CEX2.1). The PMMA part is glued to the glass slide with Dichloromethane (Carl Roth: Art. No. 8424.2). We use platinum wires (Merck: Art. No. 267201-400MG) with a diameter of 0.5 mm as electrodes. The electrode mounting is milled from a 10 mm PMMA sheet. We use a standard Xbox Controller (PDP 049-012-EU-RD Controller Xbox Series X Rot) connected via an USB-cable to the microscope computer to control electrical signals generated by the sound card of the computer. A more detailed description, including photographs of the setup, can be found in the Supplementary Materials. For microscopy, we used an Olympus IX71 inverted microscope equipped with a 20x objective (Olympus UPlanFL N 20x/0.50) and an 100x objective (Olympus PlanApo 100x/1.40 Oil). During our screening experiments we monitored the current and voltage with a digital oscilloscope (PicoScope 2000) to avoid systematic errors. Electric signals for our screening experiments were created with a function generator (RIGOL DG812) and amplified with an amplifier built in-house.

Acknowledgments

We thank Thomas Mayer for helping us with the DNA strand design. We thank Jonathan List for providing the second stage of our custom-built amplifiers.

Funding:

This work was funded by the Deutsche Forschungsgemeinschaft (DFG, German Research Foundation) Project-ID 364653263 TRR 235. We acknowledge additional support via the Excellence Strategy of the Federal Government and the Länder through the TUM Innovation Network Robotic Intelligence in the Synthesis of Life (RISE).

Author contributions:

F.K. and F.C.S. conceived the project. F.K. planned the experiments, built the experimental setup, performed all experiments, and analyzed the data. F.K. wrote the paper with support by F.C.S.

References

[1] Robert W. Johnstone and M. Parameswaran. Microscale physics. In Robert W. Johnstone and M. Parameswaran, editors, *An Introduction to Surface-Micromachining*, Springer eBook Collection, pages 45–62. Springer US, Boston, MA and s.l., 2004.

[2] Eric Lauga and Thomas R. Powers. The hydrodynamics of swimming microorganisms. *Reports on Progress in Physics*, 72(9):096601, 2009.

[3] Walter F. Paxton, Kevin C. Kistler, Christine C. Olmeda, Ayusman Sen, Sarah K. St Angelo, Yanyan Cao, Thomas E. Mallouk, Paul E. Lammert, and Vincent H. Crespi. Catalytic nanomotors: autonomous movement of striped nanorods. *Journal of the American Chemical Society*, 126(41):13424–13431, 2004.

[4] Timothy R. Kline, Walter F. Paxton, Thomas E. Mallouk, and Ayusman Sen. Catalytic nanomotors: remote-controlled autonomous movement of striped metallic nanorods. *Angewandte Chemie (International ed. in English)*, 44(5):744–746, 2005.

[5] Jared Burdick, Rawiwan Laocharoensuk, Philip M. Wheat, Jonathan D. Posner, and Joseph Wang. Synthetic nanomotors in microchannel networks: directional microchip motion and controlled manipulation of cargo. *Journal of the American Chemical Society*, 130(26):8164–8165, 2008.

[6] Florian Katzmeier, Bernhard Altaner, Jonathan List, Ulrich Gerland, and Friedrich C. Simmel. Emergence of colloidal patterns in ac electric fields. *Physical Review Letters*, 128(5):058002, 2022.

[7] Raúl Fernández-Mateo, Pablo García-Sánchez, Víctor Calero, Hywel Morgan, and Antonio Ramos. Stationary electro-osmotic flow driven by ac fields around charged dielectric spheres. *Journal of Fluid Mechanics*, 924, 2021.

[8] Raúl Fernández-Mateo, Víctor Calero, Hywel Morgan, Pablo García-Sánchez, and Antonio Ramos. Wall repulsion of charged colloidal particles during electrophoresis in microfluidic channels. *Physical Review letters*, 128(7):074501, 2022.

[9] Sumit Gangwal, Olivier J. Cayre, Martin Z. Bazant, and Orlin D. Velev. Induced-charge electrophoresis of metallodielectric particles. *Physical Review Letters*, 100(5):058302, 2008.

[10] Fuduo Ma, Xingfu Yang, Hui Zhao, and Ning Wu. Inducing propulsion of colloidal dimers by breaking the symmetry in electrohydrodynamic flow. *Physical Review Letters*, 115(20):208302, 2015.

[11] Alicia Boymelgreen, Gilad Yossifon, and Touvia Miloh. Propulsion of active colloids by self-induced field gradients. *Langmuir*, 32(37):9540–9547, 2016.

[12] Ahmet F. Demirörs, Mehmet Tolga Akan, Erik Poloni, and André R. Studart. Active cargo transport with janus colloidal shuttles using electric and magnetic fields. *Soft Matter*, 14(23):4741–4749, 2018.

[13] Xingrui Zhu, Yan Gao, Ramona Mhana, Tao Yang, Benjamin L. Hanson, Xingfu Yang, Jingjing Gong, and Ning Wu. Synthesis and propulsion of magnetic dimers under orthogonally applied electric and magnetic fields. *Langmuir*, 37(30):9151–9161, 2021.

[14] Alicia M. Boymelgreen, Tov Balli, Touvia Miloh, and Gilad Yossifon. Active colloids as mobile microelectrodes for unified label-free selective cargo transport. *Nature Communications*, 9(1):760, 2018.

[15] Xiaoye Huo, Yue Wu, Alicia Boymelgreen, and Gilad Yossifon. Analysis of cargo loading modes and capacity of an electrically-powered active carrier. *Langmuir*, 36(25), 2019.

[16] Todd M. Squires and Martin Z. Bazant. Induced-charge electro-osmosis. *Journal of Fluid Mechanics*, 509:217–252, 2004.

[17] Todd M. Squires and Martin Z. Bazant. Breaking symmetries in induced-charge electro-osmosis and electrophoresis. *Journal of Fluid Mechanics*, 560:65, 2006.

[18] Dennis C. Prieve, Paul J. Sides, and Christopher L. Wirth. 2-d assembly of colloidal particles on a planar electrode. *Current Opinion in Colloid & Interface Science*, 15(3):160–174, 2010.

[19] W. D. Ristenpart, I. A. Aksay, and D. A. Saville. Electrohydrodynamic flow around a colloidal particle near an electrode with an oscillating potential. *Journal of Fluid Mechanics*, 575:83–109, 2007.

[20] F.A Morrison. Electrophoresis of a particle of arbitrary shape. *Journal of Colloid and Interface Science*, 34(2):210–214, 1970.

[21] Yue Hu, J. L. Glass, A. E. Griffith, and Seth Fraden. Observation and simulation of electrohydrodynamic instabilities in aqueous colloidal suspensions. *The Journal of Chemical Physics*, 100(6):4674–4682, 1994.

[22] Thomas B. Jones. *Electromechanics of Particles*. Cambridge University Press, 2009.

[23] VN Shilov, AV Delgado, F Gonzalez-Caballero, and C Grosse. Thin double layer theory of the wide-frequency range dielectric dispersion of suspensions of non-conducting spherical particles including surface conductivity of the stagnant layer. *Colloids and Surfaces A: Physicochemical and Engineering Aspects*, 192(1-3):253–265, 2001.

[24] Constantino Grosse. Generalization of a classic theory of the low frequency dielectric dispersion of colloidal suspensions to electrolyte solutions with different ion valences. *The Journal of Physical Chemistry B*, 113(32):11201–11215, 2009.

[25] Ben Ng and Peter H. Barry. The measurement of ionic conductivities and mobilities of certain less common organic ions needed for junction potential corrections in electrophysiology. *Journal of Neuroscience Methods*, 56(1):37–41, 1995.

[26] Yu Bai, Max Greenfeld, Kevin J. Travers, Vincent B. Chu, Jan Lipfert, Sebastian Doniach, and Daniel Herschlag. Quantitative and Comprehensive Decomposition of the Ion Atmosphere around Nucleic Acids. *Journal of the American Chemical Society*, 129(48):14981–14988, 12 2007.

[27] Elizabeth Rowatt and Robert J.P. Williams. The binding of polyamines and magnesium to dna. *Journal of Inorganic Biochemistry*, 46(2):87–97, 1992.

[28] Ory Schnitzer, Roman Zeyde, Irad Yavneh, and Ehud Yariv. Weakly nonlinear electrophoresis of a highly charged colloidal particle. *Physics of Fluids*, 25(5):052004, 2013.

[29] Ory Schnitzer and Ehud Yariv. Macroscale description of electrokinetic flows at large zeta potentials: nonlinear surface conduction. *Physical Review E*, 86(2 Pt 1):021503, 2012.

[30] D. Sehgal and I. K. Vijay. A method for the high efficiency of water-soluble carbodiimide-mediated amidation. *Analytical biochemistry*, 218(1):87–91, 1994.

[31] N. Nakajima and Y. Ikada. Mechanism of amide formation by carbodiimide for bioconjugation in aqueous media. *Bioconjugate chemistry*, 6(1):123–130, 1995.

[32] Joseph N. Zadeh, Conrad D. Steenberg, Justin S. Bois, Brian R. Wolfe, Marshall B. Pierce, Asif R. Khan, Robert M. Dirks, and Niles A. Pierce. Nupack: Analysis and design of nucleic acid systems. *Journal of computational chemistry*, 32(1):170–173, 2011.

[33] Jean-Yves Tinevez, Nick Perry, Johannes Schindelin, Genevieve M. Hoopes, Gregory D. Reynolds, Emmanuel Laplantine, Sebastian Y. Bednarek, Spencer L. Shorte, and Kevin W. Eliceiri. Trackmate: An open and extensible platform for single-particle tracking. *Methods*, 115:80–90, 2017.

[34] https://shotcut.org/.

[35] Enzo Kopperger, Jonathan List, Sushi Madhira, Florian Rothfischer, Don C. Lamb, and Friedrich C. Simmel. A self-assembled nanoscale robotic arm controlled by electric fields. *Science (New York, N.Y.)*, 359(6373):296–301, 2018.